scientific reports

Check for updates

OPEN

Enhancement of aragonite mineralization with a chelating agent for CO_2 storage and utilization at low to moderate temperatures

Jiajie Wang✉, Noriaki Watanabe✉, Kosuke Inomoto, Masanobu Kamitakahara, Kengo Nakamura, Takeshi Komai & Noriyoshi Tsuchiya

Among the $CaCO_3$ polymorphs, aragonite demonstrates a better performance as a filler material in the paper and plastic industries. Despite being ideal from the environmental protection perspective, the production of aragonite particles via CO_2 mineralization of rocks is hindered by the difficulty in achieving high production efficiencies and purities, which, however, can be mitigated by exploiting the potential ability of chelating agents on metal ions extraction and carbonation controlling. Herein, chelating agent *N*,*N*-dicarboxymethyl glutamic acid (GLDA) was used to enhance the extraction of Ca from calcium silicate and facilitate the production of aragonite particles during the subsequent Ca carbonation. CO_2 mineralization was promoted in the presence of 0.01–0.1 M GLDA at ≤ 80 °C, with the maximal $CaCO_3$ production efficiency reached 308 g/kg of calcium silicate in 60 min using 0.03 M GLDA, which is 15.5 times higher than that without GLDA. In addition, GLDA showed excellent effects on promoting aragonite precipitation, e.g., the content of aragonite was only 5.1% in the absence of GLDA at 50 °C, whereas highly pure (> 90%, increased by a factor of 18) and morphologically uniform aragonite was obtained using ≥ 0.05 M GLDA under identical conditions. Aragonite particle morphologies could also be controlled by varying the GLDA concentration and carbonation temperature. This study proposed a carbon-negative aragonite production method, demonstrated the possibility of enhanced and controlled aragonite particle production during the CO_2 mineralization of calcium silicates in the presence of chelating agents.

Given the importance of $CaCO_3$ as a filler/extender for the production of paper, paints, plastics, food, pharmaceuticals, and cosmetics[1,2], much attention has been drawn to the synthesis of high-purity $CaCO_3$ particles with controlled crystallographic and morphological characteristics[3,4]. Aragonite is the best filler material among the three $CaCO_3$ polymorphs (calcite, aragonite, and vaterite) for paper and plastics industries, and a more useful additive for the biomedical industry[3,5–8]. At present, $CaCO_3$ particles are produced using the lime-soda process, the $CaCl_2$ (Solvay) process, or carbonation, during which CO_2 is bubbled into a solution of $Ca(OH)_2$. Carbonation is a relatively environmentally friendly and potentially carbon neutral process, as $Ca(OH)_2$ is commonly prepared by heating limestone ($CaCO_3$), which is accompanied by the release of CO_2 ($CaCO_3 \rightarrow CaO + CO_2$; $CaO + H_2O \rightarrow Ca(OH)_2$; $Ca(OH)_2 + CO_2 \rightarrow CaCO_3 + H_2O$)[4,9].

The continuous increase in global CO_2 emissions has drawn much interest to the permanent storage of CO_2 via its mineralization through reactions with metal (e.g., Ca and Mg) ions extracted from silicate minerals (e.g., $CaSiO_3$) or solid wastes (e.g., steelmaking slags and municipal solid waste incinerator ashes)[10–12]. Production of $CaCO_3$ particles via CO_2 mineralization is ideal from the environmental protection perspective since this process could be negative CO_2 emissions. However, despite the abundance of CO_2 mineralization strategies (e.g., pH-swing), most of them focus on rock dissolution or CO_2 mineralization kinetics[13,14], leaving the control of the crystallographic and morphological characteristics of the as-produced carbonates underexplored. In most cases, calcite is easily precipitated as the most stable phase of $CaCO_3$[15,16], while the precipitation of the metastable

Graduate School of Environmental Studies, Tohoku University, Aramaki, Aoba-ku, Sendai 9808579, Japan. ✉email: wang.jiajie.e4@tohoku.ac.jp; noriaki.watanabe.e6@tohoku.ac.jp

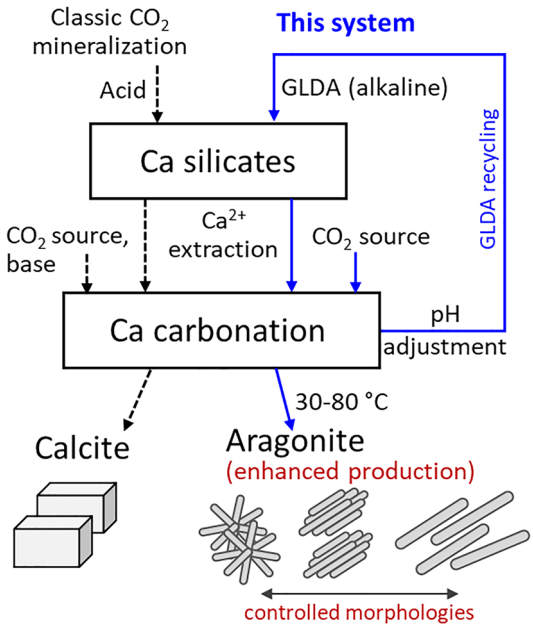

Figure 1. Schematics of GLDA-assisted aragonite production and comparison with a classic CO_2 mineralization process.

aragonite is challenging and usually requires elevated temperatures (e.g., > 75 °C) and strict pH condition (e.g., pH 11), as well as other solution chemical properties control[9,15,17], or the presence of water-soluble additives (e.g., inorganic metal ions, surfactants, and polymers)[18–20].

Chelating agents, which effectively bind metals within a wide pH range and offer considerable versatility in industrial and household uses[21,22], can also promote the extraction of metals from silicate minerals[23,24], e.g., ethylenediaminetetraacetic acid (EDTA) can significantly enhance Mg extraction from serpentine [$Mg_3Si_2O_5(OH)_4$] at pH 7 or 10[24]. Therefore, in CO_2 mineralization processes, chelating agents may enhance the production of $CaCO_3$ by promoting Ca extraction from rocks. However, the generally strong bonding between metal ions and chelating agents may prevent Ca carbonation proceeds in the presence of these agents[25].

Chelating agents may also influence $CaCO_3$ crystallization behavior by changing the surface energy of the solvent-$CaCO_3$ crystal interface[18,26,27]. Sun et al. (2014) suggested that the nucleation of the metastable aragonite can be promoted by lowering the interfacial energy[16]. However, different chelating agents may have different effects on interfacial energy. Westin and Rasmuson (2005) reported that the inclusion of chelating agents such as EDTA notably increased the interfacial energy[26], whereas Townsend et al. (2018) reported that nitrilotriacetamide (NTAA), methylglycine diacetamide (MGDA), and *N,N*-dicarboxymethyl glutamic acid (GLDA) decreased the interfacial energy and thus promoted the precipitation of acicular NaCl crystals[28]. On the other hand, the complexation of Ca ions by chelating agents results in a gradual release of these ions during carbonation and, hence, in a low Ca^{2+}/CO_3^{2-} ratio. Tomiyama and Yasushi (1984) suggested that low Ca^{2+}/HCO_3^{2-} ratios favor the precipitation of aragonite over that of calcite[29].

Herein, a chelating agent was used to enhance aragonite production during CO_2 mineralization, with the system design shown in Fig. 1. GLDA was chosen because of its biodegradability, environmental friendliness, and its good ability to chelate Ca (Ca-GLDA stability constant (log K) = 5.9 at an ionic strength of 0.1 M and 25 °C[30]) and lower the surface energy of the solvent-crystal interface for aragonite production[31]. In particular, GLDA was supposed to enhance Ca extraction from calcium silicate, promote the production of aragonite particles with controlled morphologies during the subsequent Ca carbonation, and subsequently be recovered. GLDA concentration, carbonation temperature, and pH were optimized to maximize the aragonite production efficiency as well as the purity and uniformity of aragonite particles.

Materials and methods

Materials. GLDA tetrasodium salt (GLDA-4Na, $C_9H_9NNa_4O_8$) solutions with different concentrations were prepared by mixing the initial GLDA-4Na solution (40 wt% in water, Tokyo Chemical Industry, Japan) with Milli-Q water, and pH was adjusted from an initial value of 13.8–~9.0 through the addition of aqueous HNO_3 (60–61%, Kanto Chemical, Japan). This weakly alkaline pH was used at the beginning of the Ca extraction process to minimize the cost of pH regulation, as subsequent $CaCO_3$ precipitation requires alkaline environments (pH > 8)[32,33]. High-purity commercial calcium silicate powders (Fig. 2, < 30 μm) with a general composition of $CaSiO_3$ (Wako Pure Chemical Industries, Japan) were used as a Ca source to represent silicate minerals. Na_2CO_3 (>99.0%, Kanto Chemical, Japan), $NaHCO_3$ (> 99.0%, Kanto Chemical, Japan), and CO_2 gas (> 99.995 vol.%, Taiyo Nippon Sanso, Japan) were used as CO_2 sources to optimize the $CaCO_3$ production system.

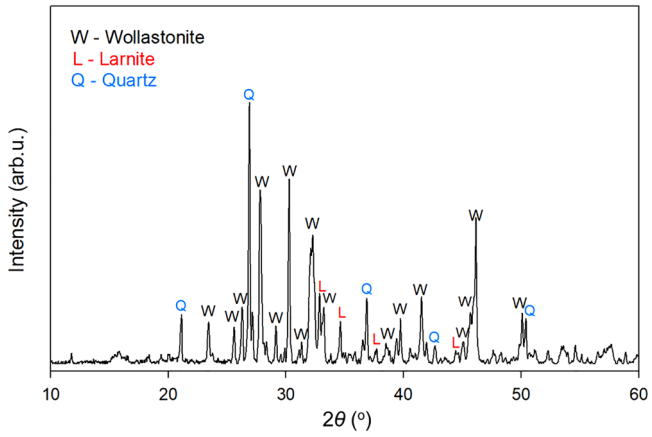

Figure 2. Representative X-ray diffraction (XRD) pattern of the employed calcium silicate.

Experiment design. All reactions were conducted in beakers. In the first step, calcium silicate powders (1.16 g) were suspended in GLDA solutions (100 mL; 0, 0.01, 0.03, 0.05, 0.10, and 0.30 M) to achieve a calcium silicate concentration of 0.1 M, and the suspensions were continuously stirred (300 rpm) for 20 min at 50 °C. This slightly-higher-than-ambient temperature was selected to accelerate Ca extraction[14]. Samples (~ 1 mL) were withdrawn after 0, 2, 5, 10, and 20 min using a syringe.

The suspensions were filtered through 0.45-µm membranes to remove residual calcium silicate particles, and the obtained transparent GLDA solutions (Ca-rich) were treated with solid Na_2CO_3, solid $NaHCO_3$, or CO_2 gas at 30, 50, or 80 °C to trigger Ca carbonation. In the case of using CO_2 gas for Ca carbonation, high purity CO_2 gas (> 99.995 vol.%) were injected into the Ca-rich GLDA solutions by bubbling, the flow rate was not recorded in this study. All carbonation experiments were conducted at the atmospheric pressure. Each carbonation experiment was conducted with continuous stirring at 200 rpm for 60 min, with samples (~ 1 mL) withdrawn via a syringe after 20, 40, and 60 min. The total volume of extracted samples was below 10% of the initial GLDA solution volume, and the sampling procedure was therefore assumed to have no major effects on the reactions. After carbonation, the suspensions were filtered through 0.45-µm membranes, and the obtained $CaCO_3$ precipitates were analyzed.

Analytical methods. Solution pH before and after each reaction was measured using a pH meter at room temperature (~ 20 °C). Fluid samples were analyzed by inductively coupled plasma-optical emission spectrometry (ICP-OES; Agilent 5100) to quantify the dissolved components (i.e., Ca and Si). The solid samples collected after Ca carbonation were filtered, washed with Milli-Q water, and dried at 50 °C for > 24 h before measurements. Crystal structures were identified by XRD (Multiflex, Rigaku, Japan) at 40 kV and 15 mA using Cu K_α radiation, a 2θ range of 10°–60°, and a scan step of 0.02°, and the acquired data were analyzed using MDI Jade 6 software[19]. Surface morphologies were characterized by SEM (SU-8000, Hitachi, Japan) coupled with energy-dispersive X-ray spectroscopy (EDS). Crystallite sizes were estimated using MDI Jade 6 software according to the Scherrer equation. Instrumental broadening and crystallinity were not considered, as they were supposed not to influence the crystallite variation trend[9,20]. Particle sizes were determined using SEM.

Results and discussion

GLDA-enhanced Ca extraction from calcium silicate. In all experiments, Ca extraction was almost complete in 20 min. The faster Ca extraction at the beginning may be attributed to the dissolution of smaller calcium silicate particles, as suggested by Gadikota et al. (2014), that silicate particles smaller than 10 µm dissolved much faster than coarser particles[34]. However, according to SEM imaging, extraction had no obvious effect on the appearance of calcium silicate particles (Fig. 3). The difficulty in size observation may be related with both the aggregation effects and the overall decrease in particle size.

The extraction conditions and solution chemistries obtained after 20 min were summarized in Table 1 and Fig. 4. The Ca extraction efficiency of 41.64% reached after 20-min treatment with 0.03 M GLDA was 17.9 times higher than that obtained without GLDA under identical conditions (2.33%). Given that one chelating agent molecule usually binds to one metal ion, the Ca/GLDA molar ratio of 1.39 observed for 0.03 M GLDA implied that almost all GLDA molecules were used for Ca bonding. However, with a further increase in GLDA concentration to 0.3 M, the Ca extraction efficiency did not increase, and the Ca/GLDA molar ratio decreased to 0.15, which suggested that the main factor preventing the improvement of Ca extraction efficiency was the change in $CaSiO_3$ particle properties. For instance, an incongruent dissolution of Ca and Si (Ca/Si in solution ≥ 2.06) was observed, i.e., the dissolution of Ca was preferred, while Si preferentially remained on the calcium silicate surface (Table 1). When the GLDA concentration was decreased from 0.03 to 0.01 M, the Ca extraction efficiency dramatically decreased to 14.66% (Table 1), and the Ca/GLDA molar ratio reached 1.47, i.e., extraction was hindered by the insufficient amount of GLDA. Therefore, a GLDA level of 0.03 M was concluded to

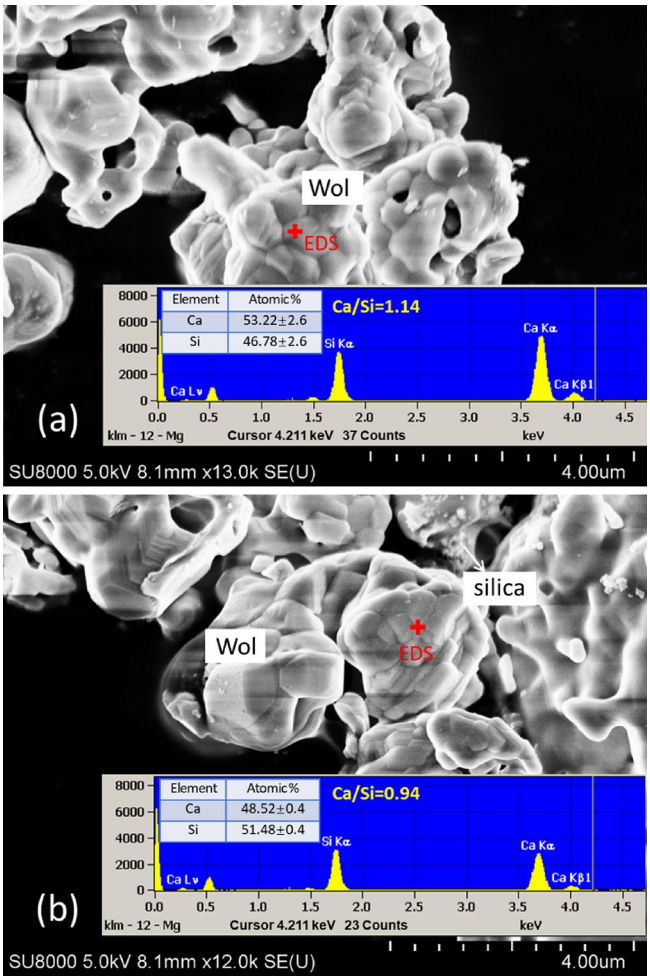

Figure 3. SEM images and EDS results of calcium silicate particles (**a**) before and (**b**) after 20 min treatment with 0.3 M GLDA. Wol: wollastonite.

Exp.	GLDA (M)	pH_0 [b]	pH_d [b]	Ca extraction (mM, or %)	Si extraction (mM, or %)	Ca/Si mol/mol	Ca/GLDA mol/mol
1	0	9.1	11.7	2.33	0.53	4.46	–
2	0.01	9.0	12.0	14.66	4.21	3.51	1.47
3	0.03	8.9	12.3	41.64	19.63	2.12	1.39
4	0.05	9.0	11.9	41.75	20.26	2.06	0.83
5	0.10	9.0	10.0	46.25	21.89	2.12	0.46
6	0.30	9.0	9.3	45.96	2.84	16.73	0.15

Table 1. Conditions of the calcium silicate-GLDA reaction and fluid chemistries obtained after 20-min extraction.[a] [a]All experiments were conducted with 0.1 M Ca silicate at 50 °C. Each experiment was repeated twice and the average values were shown, the experiments showed good reproducibility within a margin of error of 3%. [b]"pH_0" refers to the initial pH, and "pH_d" refers to the pH after dissolution. Both pH values were measured at room temperature.

be optimal for the extraction of Ca from 0.1 M calcium silicate. At this GLDA concentration, the levels of both GLDA-bonded and free Ca ions were maximized.

The extraction efficiencies of Si were lower than those of Ca, as the Ca/Si molar ratio in the solution was greater or equal to 2.06 in all cases (Table 1). EDS measurement of the surface of calcium silicate particles also revealed a slightly decrease in Ca/Si ratio from 1.14 to 0.94 after 20 min treatment with 0.3 M GLDA (Fig. 3). Nevertheless, more Si was extracted with ≥ 0.03 M GLDA than in its absence, which implies that this chelating agent can suppress the formation of a silica-rich layer to some extent to facilitate the release of Ca from calcium silicate. The formation of silica-rich passivating layers (with thicknesses ranging from several nm to μm) has been

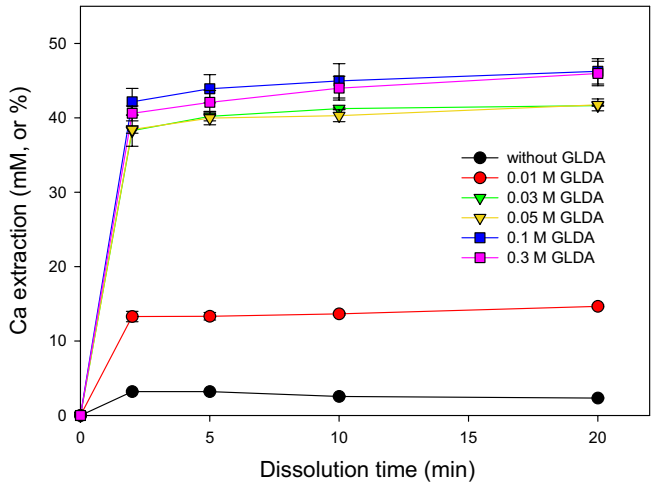

Figure 4. The changes of Ca concentrations (or extraction ratio, %) with dissolution time in the presence of 0–0.3 M GLDA.

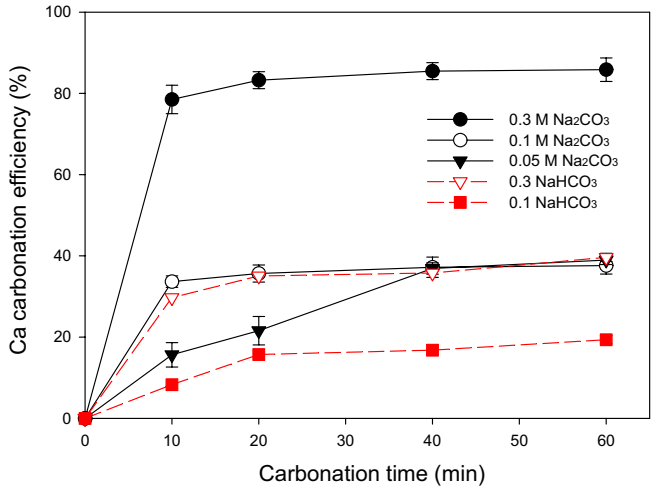

Figure 5. Effects of time and carbonation agent type/concentration on Ca carbonation efficiency. Carbonation experiments with Na_2CO_3 addition were repeated twice and the average values were shown.

considered as one of the major contributors to the suppressed dissolution of metal ions from silicate minerals during CO_2 mineralization[12,35].

In all experiments, pH increased after 20-min extraction (Table 1), which was ascribed to silicate dissolution or/and chelation[24,36–38]. Generally, GLDA concentration was negatively correlated with the extent of pH change, which was attributed to the buffering effect of $GLDA^{4+}$ and $H\text{-}GLDA^{3+}$. In the case of 0.3 M GLDA, pH increased from 9.0 to 9.3 over 20 min. At this pH, the solubility of SiO_2 is low, and the released SiO_2 may be precipitated, which may explain the low concentration of Si in the solution (Table 1, Exp. 6).

Feasibility of aragonite production in the presence of GLDA. The feasibility of $CaCO_3$ production in the presence of GLDA was studied using the extract obtained using 0.03 M GLDA (Exp. 3, Table 1; Ca/GLDA = 1.39) and containing 41.64 mM extracted Ca. Excessive Na_2CO_3 (0.05–0.3 M), $NaHCO_3$ (0.1–0.3 M), and CO_2 gas were then added to promote Ca carbonation and aragonite production at an elevated temperature of 80 °C[19]. The Ca carbonation efficiency (carbonated Ca/extracted Ca) was determined by assuming that the decrease in Ca concentration was exclusively caused by Ca carbonation.

In most cases, Ca carbonation was fast in the first 20 min but rapidly slowed down in the following period (Fig. 5), as indicated by the rapid decrease in Ca concentration. Carbonation was enhanced by high CO_3^{2-} concentrations, and the maximal efficiency of 85.84% was achieved using the highest Na_2CO_3 level of 0.3 M. At a lower CO_3^{2-} concentration of 0.1 M, which was still excessive for Ca carbonation, the Ca carbonation efficiency decreased to 37.61% (Fig. 5). Notably, pH was not influenced by Na_2CO_3 concentration (Table 2).

One the other hand, the addition of 0.1 and 0.3 M $NaHCO_3$ reduced the solution pH from 12.3 to 9.7 and 9.2, respectively, and severely suppressed carbonation, and Ca carbonation efficiencies of 19.36 and 39.62%,

GLDA (M)	Na_2CO_3 (M)	*T* (°C)	pH_c[a]	Phase content (%)[b]			Crystallite size of aragonite (nm)[b]					
							Crystallite orientation					
				A	C	V	111	021	012	200	221	Mean
0.03	0.3	80	12.3	83.2	16.8	–	58.9	58.8	72.9	45.3	58.0	58.8
0.03	0.1	80	12.3	93.3	6.7	–	30.7	29.9	34.4	22.8	32.0	30.0
0.03	0.05	80	12.4	55.1	44.9	–	18.7	17.0	24.4	–	17.3	19.4
$NaHCO_3$ (M)												
0.03	0.3	80	9.2	100	–	–	33.8	22.7	27.2	15.3	23.7	24.5
0.03	0.1	80	9.7	97.2	2.8	–	29.9	20.9	22.7	14.3	32.0	22.5

Table 2. Selected parameters of $CaCO_3$ particles obtained under various carbonation conditions. A: aragonite, C: calcite, V: vaterite. [a] pH_c refers to the pH measured after 60-min carbonation. [b] Phase compositions and aragonite crystallite sizes were determined from XRD data using MDI Jade 6.

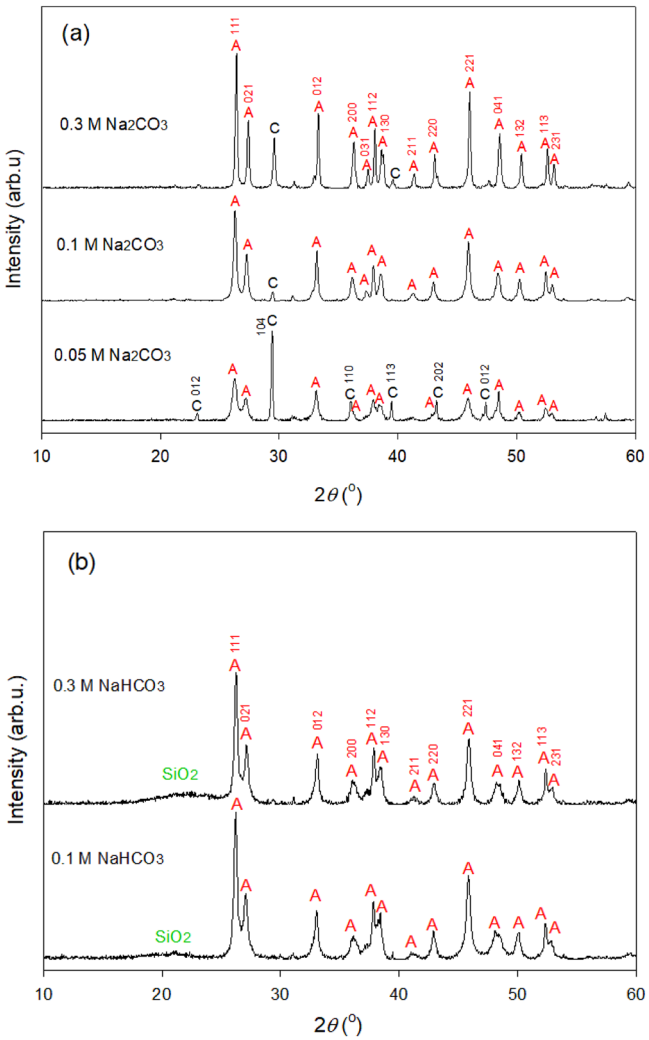

Figure 6. XRD patterns of $CaCO_3$ precipitated during carbonation with (**a**) 0.05–0.3 M Na_2CO_3 and (**b**) 0.1–0.3 M $NaHCO_3$ in 0.03 M GLDA at 80 °C.

respectively, were obtained after 60 min (Fig. 5). Direct CO_2 injection did not trigger Ca carbonation and no obvious precipitation was observed even when the pH was decreased from 12.3 to 7.0 by CO_2 bubbling, which was attributed to the low concentration of dissolved CO_2. Thus, to effectively utilize CO_2 gas for Ca carbonation, the pH should be kept alkaline before a sufficient CO_2 concentration is reached.

Higher CO_3^{2-} concentrations favored aragonite formation, as suggested by the increase in the intensity of aragonite XRD peaks (Fig. 6a). For instance, as the CO_3^{2-} concentration increased from 0.05 to 0.3 M, the raw

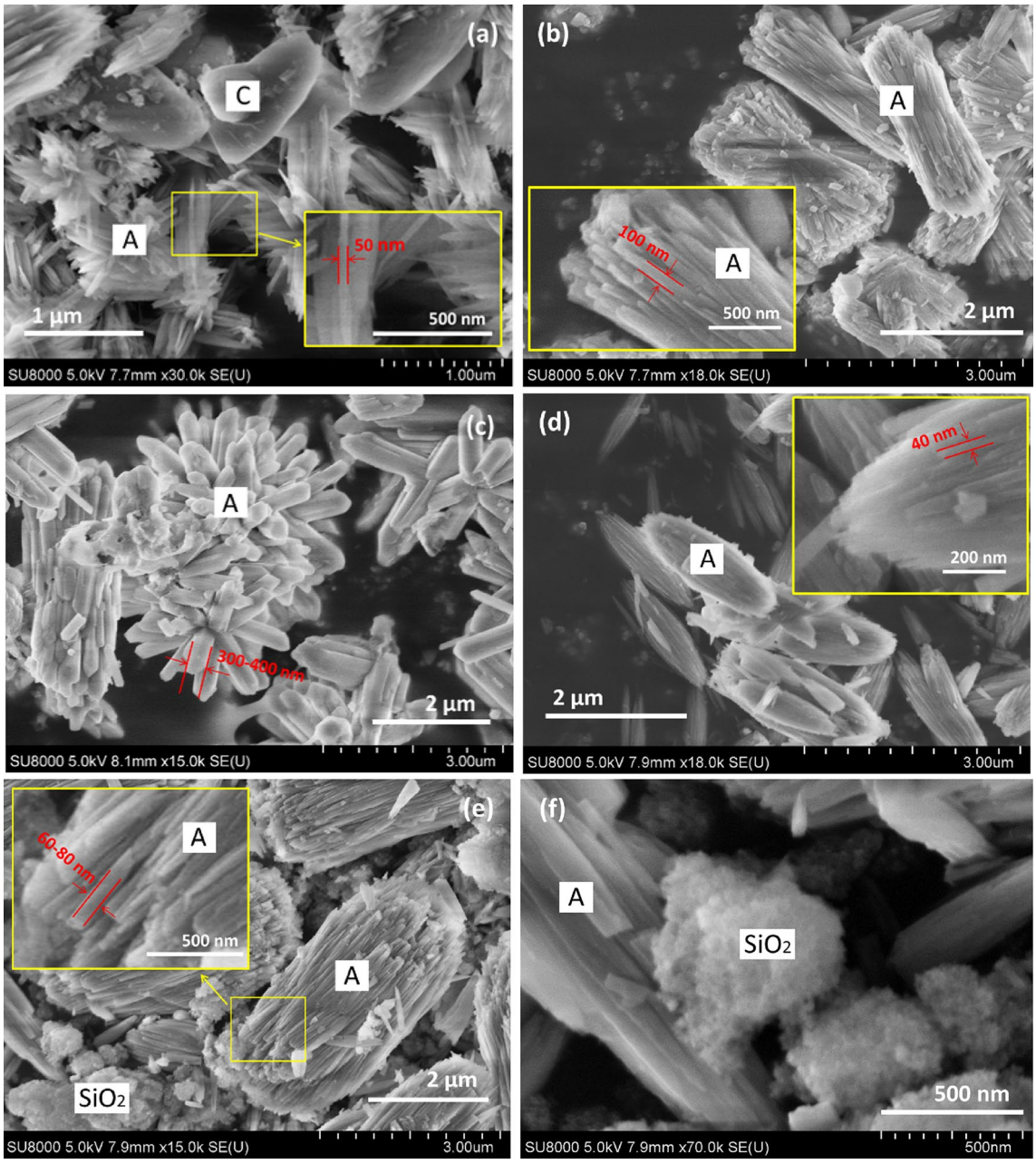

Figure 7. SEM images of $CaCO_3$ particles produced using (**a**, **b**) 0.05 M Na_2CO_3, (**c**) 0.1 M Na_2CO_3; (**d**) 0.3 M Na_2CO_3, (**e**) 0.1 M $NaHCO_3$, and (**f**) 0.3 M $NaHCO_3$ in 0.03 M GLDA (obtained after Exp. 3 in Table 1) at 80 °C.

intensity of aragonite peak observed at 26.2° increased from 693 to 2215 arb.u. The fast precipitation of $CaCO_3$ with the preferred generation of aragonite was consistent with the results of Hirano et al. (2009)[39]. Table 2 lists the mean crystallite sizes determined using 111, 021, 012, 200, and 221 peaks and reveals that high Na_2CO_3 concentrations increased crystallite size irrespective of the orientation used for measurement. In particular, as the Na_2CO_3 concentration increased from 0.05 to 0.3 M, the mean crystallite size increased from 19.4 to 58.8 nm, and the width of aragonite particles increased from ~ 50 to 300–400 nm (Fig. 7a–c). The fact that aragonite particles were larger than the corresponding crystallites implies that these particles were made up of several different crystallites[40]. Thus, high CO_3^{2-} concentrations favored aragonite crystallization and nucleation in the presence of GLDA.

The characteristic XRD peaks of calcite became weaker when the concentration of CO_3^{2-} increased from 0.05 to 0.1 M but gained intensity as the CO_3^{2-} concentration further increased to 0.3 M (Fig. 6a). The aragonite-to-calcite ratios of each solid sample were semi-determined using MDI Jade 6 under the assumption that all carbonation products were crystalline and detectable by XRD (Table 2). The highest aragonite content of 93.3% was achieved using 0.1 M Na_2CO_3, which may be associated with the contradictory effects of CO_3^{2-} concentration on aragonite (or calcite) formation. A higher CO_3^{2-} concentration may enhance the production of calcite[3] but a

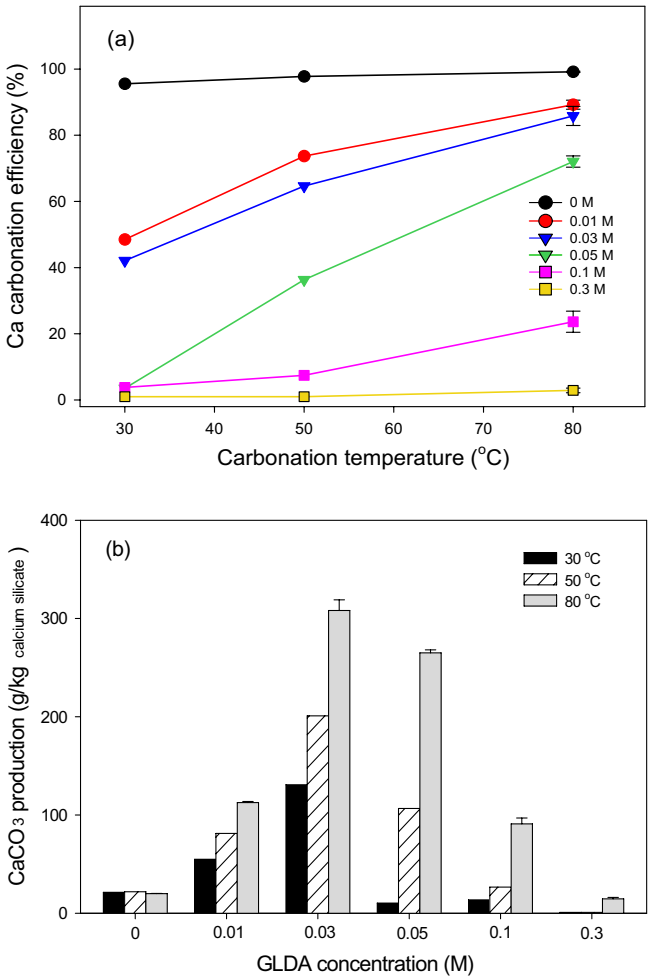

Figure 8. Effects of temperature and GLDA concentration on (**a**) the Ca carbonation efficiency obtained after 60 min using 0.3 M Na_2CO_3, and (**b**) $CaCO_3$ production efficiency. Carbonation experiments conducted at 80 °C were repeated twice and the average values were shown.

lower Ca^{2+}/CO_3^{2-} was also reported to suppress calcite formation[19,29]. If this is true, aragonite purity can be controlled by variation of the CO_3^{2-} concentration. However, this assumption was not verified in the present study.

Aragonite was the dominant $CaCO_3$ polymorph obtained at $NaHCO_3$ concentrations of 0.1–0.3 M at pH 9.2–9.7 (Fig. 6b). This finding was consistent with the results of Chang and Tai (2010), who found that low pH favors aragonite formation[41]. The produced aragonite particles had relatively small crystallite sizes (mean = 22.5–24.5 nm, Table 2) and dimensions (width = 40–80 nm, Fig. 7d,e). The suppressed aragonite growth may be attributed to low pH, while the increase in $NaHCO_3$ concentration had little effect on the enlargement of aragonite crystallites and particles. Based on the above results, low-pH GLDA solutions were expected to induce aragonite production and help to increase aragonite purity; however, an inhibition of aragonite crystallization was observed. At lower pH (e.g., pH ≤ 9.7), amorphous silica precipitation was favored, as evidenced by the broad XRD peak in the range of 15°–25° (Fig. 6b)[42] and the fine particles observed in the SEM images (Fig. 7), which decreased aragonite purity. Thus, Ca carbonation in the presence of GLDA was concluded to be feasible, and high CO_3^{2-} concentrations were found to enhance aragonite crystallization and precipitation.

GLDA-enhanced aragonite production at different temperatures. Extracts obtained using GLDA solutions with various concentrations were treated with 0.3 M Na_2CO_3 at 30–80 °C. For experiments in which $CaCO_3$ precipitation was observed (≤ 0.1 M GLDA), Ca carbonation was fast in the first 20 min but was almost complete in 60 min. Figure 8a presents the Ca carbonation efficiencies obtained after 60 min at 30–80 °C for different GLDA concentrations.

In the absence of GLDA, the carbonation efficiency remained high (> 95%) at all temperatures but significantly increased with temperature at moderate GLDA concentrations of 0.01–0.1 M, reaching 89.24% (0.01 M GLDA) and 85.84% (0.03 M GLDA) at 80 °C. This efficiency was expected to further increase at higher temperatures. Interestingly, Ca carbonation could be triggered at lower temperatures in solutions with lower GLDA concentrations. For instance, at GLDA concentrations of 0–0.03 M, a certain amount of Ca could be carbonated at 30 °C, whereas at a GLDA level of 0.3 M, Ca carbonation was difficult even at 80 °C.

Ca carbonation efficiency was closely related to the final Ca/GLDA molar ratio (i.e., that obtained after 60-min carbonation) at all temperatures. This ratio equaled 0.66 ± 0.03, 0.39 ± 0.04, and 0.19 ± 0.02 after 60-min carbonation at 30, 50, and 80 °C, respectively (the initial values are shown in Table 1), with small differences observed between various GLDA concentrations for each temperature. The decrease in the Ca/GLDA molar ratio with increasing temperature may be due to concomitant changes in parameters such as the Ca-GLDA stability constant, the $CaCO_3$ solubility constant[43], and the carbonate dissociation constant (i.e., pK_a of HCO_3^-). Changes in the carbonate dissociation constant may have small effects on $CaCO_3$ formation at pH > 12, whereas decreases in the Ca-GLDA stability constant and the $CaCO_3$ solubility constant may positively influence Ca carbonation[44] and thus promote Ca release from Ca-GLDA complexes and the precipitation of $CaCO_3$. Thus, $CaCO_3$ production during Ca carbonation can possibly be enhanced by increasing the Ca/chelating agent molar ratio during Ca extraction, adjusting the pH or rock dosage, and lowering the Ca-GLDA stability constant.

The $CaCO_3$ production per kg of calcium silicate was calculated by combining the results of Ca extraction (Table 1) and Ca carbonation (Fig. 8a), as summarized in Fig. 8b. Compared to that obtained in the absence of GLDA, significantly higher $CaCO_3$ production efficiencies were obtained for combinations of 0.01–0.03 M GLDA + carbonation temperature ≥ 30 °C, 0.05 M GLDA + carbonation temperature ≥ 50 °C, and 0.1 M GLDA + carbonation temperature ≥ 80 °C. The optimum GLDA concentration for $CaCO_3$ production from 0.1 M calcium silicate was 0.03 M, in which case the highest $CaCO_3$ production efficiency of 308 g/kg of calcium silicate was reached in ~ 20 min (35.76% of calcium silicate was carbonated) and was 15.5 times higher than that obtained without GLDA (19.9 g/kg of calcium silicate). Even higher $CaCO_3$ production efficiencies were expected at carbonation temperatures above 80 °C in the presence of GLDA. These results suggested that chelating agents can significantly enhance $CaCO_3$ production and showed that chelating agent concentration is an important factor that should be controlled at a certain low level, as otherwise, the decrease in the Ca-GLDA stability constant precludes the release of sufficient Ca for carbonation.

GLDA-controlled $CaCO_3$ crystallization behavior. In addition to affecting the $CaCO_3$ production efficiency, GLDA concentration also influenced the $CaCO_3$ precipitation behavior. At a carbonation temperature of 80 °C and high GLDA concentrations in the range of 0–0.1 M, the aragonite XRD peaks were stronger than the calcite peaks (Fig. 9a), which implied that the former polymorph was generated in preference to the latter. Upon the addition of 0.01 M GLDA, the aragonite content increased from 5.1% (without GLDA) to 62.7%, while the calcite content decreased from 94.9 to 37.3% (Table 3). When ≥ 0.05 M GLDA was used at 80 °C, the XRD pattern featured dominant aragonite peaks and no calcite peaks (Fig. 9a), i.e., high-purity aragonite particles were formed (~ 100%, Table 3). Although aragonite production requires a relatively low pH (e.g., 9), the inclusion of GLDA allowed the acceptable pH range to be significantly expanded (i.e., to 9.2–12.3)[17,41]. The increase in GLDA concentration from 0.01 to 0.1 M resulted in an increased aragonite crystallite size for all orientations (from 55.6 to 66.8 nm on average).

The inclusion of GLDA extended the temperature range for aragonite production down to 30 °C, while previous studies employed carbonation temperatures of > 75 °C[45,46]. In the case of 0.03 M GLDA, the aragonite content equaled 33.0% even at a low temperature of 30 °C (Table 3) and increased with increasing carbonation temperature, reaching 83.2% at 80 °C. However, in the absence of GLDA, aragonite contents of ≤ 5.1% were obtained at carbonation temperatures of 30–80 °C. Notably, the size of aragonite crystallites increased only at high temperatures of 50–80 °C (Table 3).

The morphologies of as-prepared $CaCO_3$ are shown in Fig. 10. At a low temperature of 30 °C, spherical vaterite particles were mainly generated in the absence of GLDA (Fig. 10a), in line with the XRD results (Fig. 9b). However, in 0.01 M GLDA, all three $CaCO_3$ polymorphs were generated (Fig. 10b). The elongated particles with three end faces on each side of the crystal were regarded as calcite, as suggested by Altay et al. (2007)[18], whereas bundles of rods were identified as aragonite[20]. Significant variations in aragonite morphology with GLDA concentration were observed. At 30 °C, an increase in GLDA concentration from 0.01 to 0.03 M promoted the clustering of aragonite rod bundles to form bouquet-like aggregates (Fig. 10c). This anisotropic aragonite crystal growth may be associated with the crystallite size increase in 111, 021, and 200 directions.

At carbonation temperatures of 50 and 80 °C, only cubic calcite particles were observed in the absence of GLDA (Fig. 10d, g). However, at a low GLDA level (e.g., 0.01 M), both aragonite and calcite were generated (Fig. 10h). At a constant temperature, the aragonite particle size was not obviously influenced by GLDA concentration in the range of 0.01–0.05 M (Table 1, Fig. 10e, f, h, i). When the GLDA concentration increased to 0.1 M, only needle-like completely separated aragonite particles were observed (Fig. 10i). The formation of these acicular particles may be closely related to the drastic increase in crystallite size in the 012 direction. Moreover, GLDA inhibited the caking of aragonite particles, which may imply a lower surface energy of aragonite[28,47]. In the presence of GLDA, Ca ions were gradually released from Ca-GLDA complexes for carbonation, and the resulting low Ca^{2+}/CO_3^{2-} ratio was considered to induce aragonite formation[29]. Thus, the enhanced formation of the metastable aragonite in the presence of GLDA was ascribed to the surface energy decrease of $CaCO_3$ particles and the low concentration of free Ca^{2+} in the solution during Ca carbonation[16].

Temperature strongly affected the morphology and size of aragonite particles. For instance, spherical particles comprising numerous aragonite rods were formed when the carbonation temperature was increased from 30 to 50 °C in 0.03 M GLDA (Fig. 10i). The high surface area of these particles makes them promising fillers for the paper industry. On the other hand, the average size of aragonite particles increased from ~100 to 300–400 nm as the temperature increased from 30 to 80 °C in 0.03 M GLDA (Fig. 10c, i), in line with the concomitant increase in aragonite crystallite size (Table 3). It should be noted that with increasing GLDA concentration, the aragonite particle size increased by larger factors than the crystallite size, which indicated that high GLDA levels promoted aragonite nucleation. Thus, we concluded that (1) GLDA can enhance aragonite formation and (2)

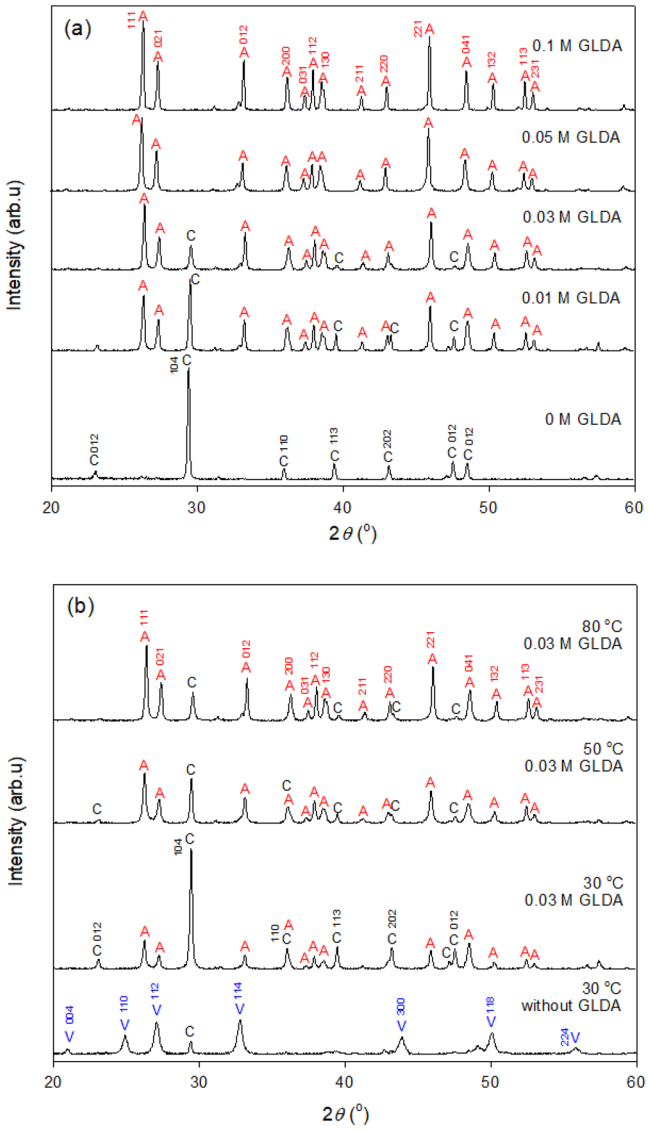

Figure 9. XRD patterns of precipitates formed during Ca carbonation (**a**) at 80 °C, GLDA concentrations of 0–0.1 M, and a Na_2CO_3 concentration of 0.3 M and (**b**) at 30–80 °C, a GLDA concentration of 0.03 M and a Na_2CO_3 concentration of 0.3 M. A: aragonite, C: calcite, V: vaterite.

GLDA (M)	Na_2CO_3 (M)	T (°C)	pH_c	Phase contents (%)			Crystallite sizes of aragonite (nm)					
							Crystallite orientation					Mean
				A	C	V	111	021	012	200	221	
0	0.3	80	11.59	5.1	94.9	–	–	–	–	–	–	–
0.01	0.3	80	11.74	62.7	37.3	–	49.9	54.6	74.0	40.2	59.3	55.6
0.03	0.3	80	12.28	83.2	16.8	–	58.9	58.8	72.9	45.3	58.0	58.8
0.05	0.3	80	11.89	100.0	–		58.2	61.9	72.1	46.4	59.6	59.6
0.1	0.3	80	10.89	100.0	–	–	72.5	74.3	90.4	65.7	66.8	66.8
0	0.3	30	10.95	–	12.0	88.0	–	–	–	–	–	–
0.03	0.3	30	12.37	33.0	67.0	–	48.0	43.9	43.1	–	57.5	48.1
0.03	0.3	50	12.32	69.2	30.8	–	45.7	40.2	43.9	–	52.4	45.6

Table 3. Effects of carbonation conditions on the selected properties of $CaCO_3$ particles. A: aragonite, C: calcite, V: vaterite

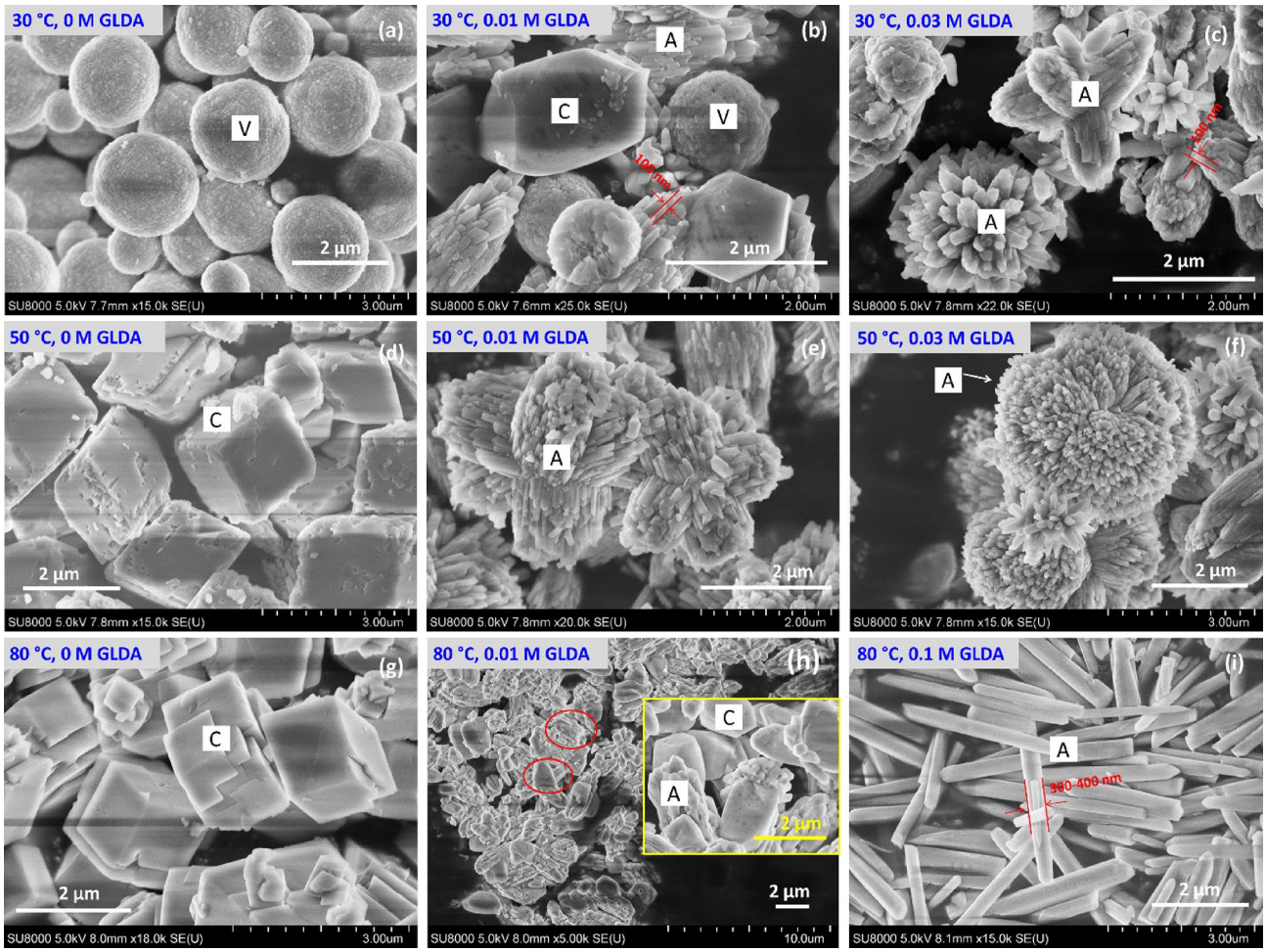

Figure 10. SEM images of $CaCO_3$ particles produced in the presence of (**a**,**d**,**g**) 0 M, (**b**,**e**,**h**) 0.01 M, (**c**,**f**) 0.03 M, and (**i**) 0.1 M GLDA at (**a**–**c**) 30 °C, (**d**–**f**) 50 °C, and (**g**–**i**) 80 °C. A: aragonite, C: calcite, V: vaterite.

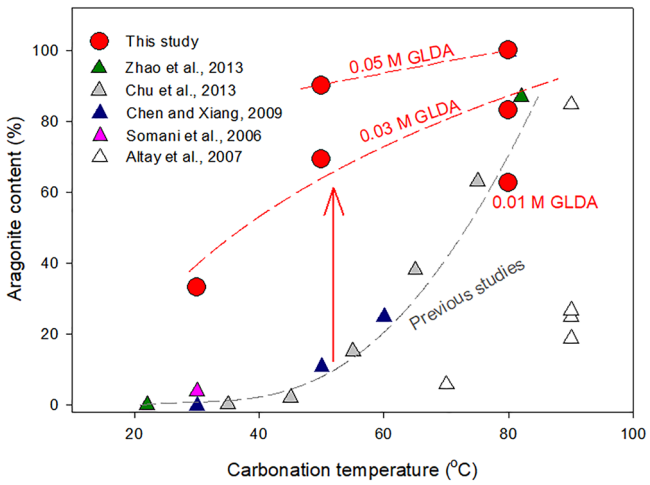

Figure 11. Effects of carbonation temperature on aragonite purity obtained in the present study and other works[3,18,19,48,49].

high-purity aragonite particles with various morphologies can be prepared by adjusting the GLDA concentration and temperature.

The effect of carbonation temperature on the aragonite content of precipitated $CaCO_3$ obtained herein and in other studies was compared in Fig. 11. Although various systems have been developed for $CaCO_3$ production, aragonite content is generally low at ≤ 70 °C. Herein, the use of 0.03 M GLDA and a carbonation temperature of 50 °C allowed us to increase the aragonite content to > 62%, which is more than seven times that obtained previously at the same temperature[3,18,19,48,49], and an even higher value of > 90% was achieved using ≥0.05 M GLDA at ≥ 50 °C. The preferential precipitation of aragonite may be associated with surface energy changes and the relatively low concentrations of free Ca^{2+} in the presence of GLDA during Ca carbonation. However, these assumptions were not experimentally verified in the present study. Production of aragonite particles via CO_2 mineralization of minerals in the presence of GLDA has the advantages of potential negative CO_2 emissions and relative low cost, the produced aragonite particles also have great application prospects in paper and plastics production owing to their high uniformity and controllable morphology[7].

Most pH-swing-based CO_2 mineralization methods require large amounts of acids and bases for rock dissolution and metal carbonation, respectively[33]. However, chelation can occur at both acidic and alkaline pH and thus help to reduce the high cost of pH regulation during CO_2 mineralization. At the same time, high-purity metastable aragonite with controllable particle morphology can be produced for various industrial purposes, thus providing additional commercial value. The developed system can be improved by injecting CO_2 gas into the spent GLDA solution to return the pH to the initial value (e.g., 9.0) and thus recover SiO_2 for GLDA recycling (Fig. 1) and further reduce the operational cost of aragonite production.

Conclusions

This study investigated the use of chelating agents to enhance and control the formation of $CaCO_3$ particles during the CO_2 mineralization of silicate minerals. The feasibility of the adopted approach was studied using GLDA as a chelating agent and calcium silicate as a representative silicate mineral.

The addition of GLDA accelerated the extraction of Ca from calcium silicate and thus increased the $CaCO_3$ production efficiency. In particular, the value of 308 g/kg of calcium silicate obtained under optimal conditions (0.03 M GLDA, pH 9) was 15.5 times higher than that obtained without GLDA. Moreover, GLDA promoted aragonite crystallization and nucleation and controlled its morphology. High-purity and size-/morphology-uniform aragonite particles were obtained in the presence of GLDA even at moderate temperatures (e.g., 50–80 °C) within a wide pH range (e.g., 9.2–12.3). For instance, almost 100% pure aragonite was obtained using ≥0.05 M GLDA at 80 °C, while a purity of only 5.1% was obtained in the absence of GLDA under the same conditions. The aragonite particle morphology could be controlled from bouquet-like to bundles of rods or separated rods, which can be used in various industrial applications.

$CaCO_3$ production through chelating agent–assisted CO_2 mineralization is of both environmental and commercial importance, offering the benefits of negative CO_2 emission, easy product control, facile operation, and low costs (given that the chelating agent can be recycled). Investigations regarding chelating agent recycling and economic costs will be conducted in a follow-up study.

Received: 23 April 2021; Accepted: 25 June 2021
Published online: 06 July 2021

References

1. Sioson, A. S., Choi, A. E. S., de Luna, M. D. G., Huang, Y.-H. & Lu, M.-C. Calcium carbonate granulation in a fluidized-bed reactor: Kinetic, parametric and granule characterization analyses. *Chem. Eng. J.* **382**, 122879. https://doi.org/10.1016/j.cej.2019.122879 (2020).
2. Donnet, M., Aimable, A., Lemaître, J. & Bowen, P. Contribution of aggregation to the growth mechanism of seeded calcium carbonate precipitation in the presence of polyacrylic acid. *J. Phys. Chem. B.* **114**, 12058–12067. https://doi.org/10.1021/jp103787p (2010).
3. Somani, R. S., Patel, K. S., Mehta, A. R. & Jasra, R. V. Examination of the polymorphs and particle size of calcium carbonate precipitated using still effluent (i.e., $CaCl_2$ + NaCl solution) of soda ash manufacturing process. *Ind. Eng. Chem. Res.* **45**, 5223–5230. https://doi.org/10.1021/ie0513447 (2006).
4. Ghiasi, M., Abdollahy, M., Khalesi, M. R. & Ghiasi, E. Control of the morphology, specific surface area and agglomeration of precipitated calcium carbonate crystals through a multiphase carbonation process. *CrystEngComm.* **22**, 1970–1984. https://doi.org/10.1039/C9CE01876J (2020).
5. Kanoje, B., Parikh, J. & Kuperkar, K. Crystallization study and morphology behaviour of calcium carbonate crystals in aqueous Surfactant-Pluronics® prototype. *J. Mater. Res. Technol.* **7**, 508–514. https://doi.org/10.1016/j.jmrt.2017.10.005 (2018).
6. Altiner, M. & Yildirim, M. Production and characterization of synthetic aragonite prepared from dolomite by eco-friendly leaching–carbonation process. *Adv. Powder Technol.* **28**, 553–564. https://doi.org/10.1016/j.apt.2016.10.024 (2017).
7. Konno, H., Nanri, Y. & Kitamura, M. Effect of NaOH on aragonite precipitation in batch and continuous crystallization in causticizing reaction. *Powder Technol.* **129**, 15–21. https://doi.org/10.1016/S0032-5910(02)00275-9 (2003).
8. Wang, L., Sondi, I. & Matijević, E. Preparation of uniform needle-like aragonite particles by homogeneous precipitation. *J. Colloid Interface Sci.* **218**, 545–553. https://doi.org/10.1006/jcis.1999.6463 (1999).
9. F. Munawaroh, L.K. Muharrami, Triwikantoro, Z. Arifin, The effect of CO_2 gas flow rate on precipitated CaCO3 formed at room temperature. In: Geneva, Switzerland, 2018: p. 020109. https://doi.org/10.1063/1.5054513.
10. Snæbjörnsdóttir, S. Ó. *et al.* Carbon dioxide storage through mineral carbonation. *Nat. Rev. Earth Environ.* **1**, 90–102. https://doi.org/10.1038/s43017-019-0011-8 (2020).
11. Wang, J., Watanabe, N., Okamoto, A., Nakamura, K. & Komai, T. Acceleration of hydrogen production during water-olivine-CO_2 reactions via high-temperature-facilitated Fe(II) release. *Int. J. Hydrog. Energy.* https://doi.org/10.1016/j.ijhydene.2019.03.119 (2019).
12. Liu, W. *et al.* CO2 mineral carbonation using industrial solid wastes: A review of recent developments. *Chem. Eng. J.* **416**, 129093. https://doi.org/10.1016/j.cej.2021.129093 (2021).

13. Yoo, K., Kim, B.-S., Kim, M.-S., Lee, J. & Jeong, J. Dissolution of magnesium from serpentine mineral in sulfuric acid solution. *Mater. Trans.* **50**, 1225–1230. https://doi.org/10.2320/matertrans.M2009019 (2009).
14. Ghoorah, M., Dlugogorski, B. Z., Balucan, R. D. & Kennedy, E. M. Selection of acid for weak acid processing of wollastonite for mineralisation of CO_2. *Fuel.* **122**, 277–286. https://doi.org/10.1016/j.fuel.2014.01.015 (2014).
15. Wang, W., Wang, G., Liu, Y., Zheng, C. & Zhan, Y. Synthesis and characterization of aragonite whiskers by a novel and simple route. *J. Mater. Chem.* **11**, 1752–1754. https://doi.org/10.1039/b100556l (2001).
16. Sun, W., Jayaraman, S., Chen, W., Persson, K. A. & Ceder, G. Nucleation of metastable aragonite $CaCO_3$ in seawater. *Proc. Natl. Acad. Sci.* **112**, 3199–3204. https://doi.org/10.1073/pnas.1423898112 (2015).
17. Chang, R. *et al.* Calcium carbonate precipitation for CO_2 storage and utilization: A review of the carbonate crystallization and polymorphism. *Front. Energy Res.* https://doi.org/10.3389/fenrg.2017.00017 (2017).
18. Altay, E., Shahwan, T. & Tanoğlu, M. Morphosynthesis of $CaCO_3$ at different reaction temperatures and the effects of PDDA, CTAB, and EDTA on the particle morphology and polymorph stability. *Powder Technol.* **178**, 194–202. https://doi.org/10.1016/j.powtec.2007.05.004 (2007).
19. Chu, D. H. *et al.* CO_2 mineralization into different polymorphs of $CaCO_3$ using an aqueous-CO_2 system. *RSC Adv.* **3**, 21722–21729. https://doi.org/10.1039/C3RA44007A (2013).
20. Guo, H. *et al.* Crystallization of aragonite $CaCO_3$ with complex structures. *Adv. Powder Technol.* **22**, 777–783. https://doi.org/10.1016/j.apt.2010.11.004 (2011).
21. Flora, S. J. S. & Pachauri, V. Chelation in metal intoxication. *Int. J. Environ. Res. Public. Health.* **7**, 2745–2788. https://doi.org/10.3390/ijerph7072745 (2010).
22. Leštan, D., Luo, C. & Li, X. The use of chelating agents in the remediation of metal-contaminated soils: A review. *Environ. Pollut.* **153**, 3–13. https://doi.org/10.1016/j.envpol.2007.11.015 (2008).
23. Declercq, J., Bosc, O. & Oelkers, E. H. Do organic ligands affect forsterite dissolution rates?. *Appl. Geochem.* **39**, 69–77. https://doi.org/10.1016/j.apgeochem.2013.09.020 (2013).
24. Bobicki, E. R., Liu, Q. & Xu, Z. Ligand-promoted dissolution of serpentine in ultramafic nickel ores. *Miner. Eng.* **64**, 109–119. https://doi.org/10.1016/j.mineng.2014.05.020 (2014).
25. Bonfils, B. *et al.* Comprehensive analysis of direct aqueous mineral carbonation using dissolution enhancing organic additives. *Int. J. Greenh. Gas Control.* **9**, 334–346. https://doi.org/10.1016/j.ijggc.2012.05.009 (2012).
26. Westin, K.-J. & Rasmuson, Å. C. Nucleation of calcium carbonate in presence of citric acid, DTPA, EDTA and pyromellitic acid. *J. Colloid Interface Sci.* **282**, 370–379. https://doi.org/10.1016/j.jcis.2004.09.071 (2005).
27. Gopi, S., Subramanian, V. K. & Palanisamy, K. Aragonite–calcite–vaterite: A temperature influenced sequential polymorphic transformation of $CaCO_3$ in the presence of DTPA. *Mater. Res. Bull.* **48**, 1906–1912. https://doi.org/10.1016/j.materresbull.2013.01.048 (2013).
28. Townsend, E. R. *et al.* Additive induced formation of ultrathin sodium chloride needle crystals. *Cryst. Growth Des.* **18**, 755–762. https://doi.org/10.1021/acs.cgd.7b01170 (2018).
29. Tomiyama, C. & Kitano, Y. Calcite formation in calcium chloride rich water. *Jpn. J. Limnol. Rikusuigaku Zasshi.* **45**, 1–5. https://doi.org/10.3739/rikusui.45.1 (1984).
30. AkzoNobel Functional Chemicals Chelates. Dissolvine GL Technical brochure - PDF Free Download, (n.d.). https://docplayer.net/48658049-Akzonobel-functional-chemicals-chelates-dissolvine-gl-technical-brochure.html (accessed August 2, 2020).
31. Bretti, C., Majlesi, K., De Stefano, C. & Sammartano, S. Thermodynamic study on the protonation and complexation of GLDA with Ca^{2+} and Mg^{2+} at different ionic strengths and ionic media at 298.15 K. *J. Chem. Eng. Data.* **61**, 1895–1903. https://doi.org/10.1021/acs.jced.6b00063 (2016).
32. Scholz, F. & Kahlert, H. The calculation of the solubility of metal hydroxides, oxide-hydroxides, and oxides, and their visualisation in logarithmic diagrams. *ChemTexts.* **1**, 7. https://doi.org/10.1007/s40828-015-0006-0 (2015).
33. Gadikota, G. Multiphase carbon mineralization for the reactive separation of CO_2 and directed synthesis of H_2. *Nat. Rev. Chem.* **4**, 78–89. https://doi.org/10.1038/s41570-019-0158-3 (2020).
34. Gadikota, G., Matter, J., Kelemen, P. & Park, A. A. Chemical and morphological changes during olivine carbonation for CO_2 storage in the presence of NaCl and $NaHCO_3$. *Phys. Chem. Chem. Phys.* **16**, 4679. https://doi.org/10.1039/c3cp54903h (2014).
35. Daval, D. *et al.* Influence of amorphous silica layer formation on the dissolution rate of olivine at 90°C and elevated pCO_2. *Chem. Geol.* **284**, 193–209. https://doi.org/10.1016/j.chemgeo.2011.02.021 (2011).
36. Haque, F., Chiang, Y. W. & Santos, R. M. Alkaline mineral soil amendment: A climate change 'stabilization wedge'?. *Energies.* **12**, 2299. https://doi.org/10.3390/en12122299 (2019).
37. Prabhakar, S., Hanumantha Rao, K. & Forsling, W. Dissolution of wollastonite and its flotation and surface interactions with tallow-1,3-diaminopropane (duomeen T). *Miner. Eng.* **18**, 691–700. https://doi.org/10.1016/j.mineng.2004.11.001 (2005).
38. Wang, J., Watanabe, N., Okamoto, A., Nakamura, K. & Komai, T. Enhanced hydrogen production with carbon storage by olivine alteration in CO_2-rich hydrothermal environments. *J. CO2 Util.* **30**, 205–213. https://doi.org/10.1016/j.jcou.2019.02.008 (2019).
39. Hirano, N., Takenoshita, A. & Tsuchiya, N. Carbonate sinter in the Oku-Okuhachikuro hot spring, Akita Prefecture-Co-existence of aragonite and calcite in calcareous sinter. *Jpn. Mag. Mineral. Petrol. Sci.* **38**, 198–207. https://doi.org/10.2465/gkk.38.198 (2009).
40. Rabiei, M. *et al.* Comparing methods for calculating nano crystal size of natural hydroxyapatite using X-ray diffraction. *Nanomaterials.* **10**, 1627. https://doi.org/10.3390/nano10091627 (2020).
41. Chang, M.-C. & Tai, C. Y. Effect of the magnetic field on the growth rate of aragonite and the precipitation of $CaCO_3$. *Chem. Eng. J.* **164**, 1–9. https://doi.org/10.1016/j.cej.2010.07.018 (2010).
42. Zainuri, M. Darminto, Synthesis of SiO_2 nanopowders containing quartz and cristobalite phases from silica sands. *Mater. Sci.-Pol.* **33**, 47–55. https://doi.org/10.1515/msp-2015-0008 (2015).
43. Weyl, P. K. The change in solubility of calcium carbonate with temperature and carbon dioxide content. *Geochim. Cosmochim. Acta.* **17**, 214–225. https://doi.org/10.1016/0016-7037(59)90096-1 (1959).
44. Coto, B., Martos, C., Peña, J. L., Rodríguez, R. & Pastor, G. Effects in the solubility of $CaCO_3$: experimental study and model description. *Fluid Phase Equilib.* **324**, 1–7. https://doi.org/10.1016/j.fluid.2012.03.020 (2012).
45. Marin Rivera, R. & Van Gerven, T. Production of calcium carbonate with different morphology by simultaneous CO_2 capture and mineralisation. *J. CO2 Util.* **41**, 101241. https://doi.org/10.1016/j.jcou.2020.101241 (2020).
46. Habte, L. *et al.* Synthesis, characterization and mechanism study of green aragonite crystals from waste biomaterials as calcium supplement. *Sustainability.* **12**, 5062. https://doi.org/10.3390/su12125062 (2020).
47. Townsend, E. R., Swennenhuis, F., van Enckevort, W. J. P., Meijer, J. A. M. & Vlieg, E. Creeping: an efficient way to determine the anticaking ability of additives for sodium chloride. *CrystEngComm.* **18**, 6176–6183. https://doi.org/10.1039/C6CE01376G (2016).
48. Zhao, H., Park, Y., Lee, D. H. & Park, A.-H.A. Tuning the dissolution kinetics of wollastonite via chelating agents for CO_2 sequestration with integrated synthesis of precipitated calcium carbonates. *Phys. Chem. Chem. Phys.* **15**, 15185–15192. https://doi.org/10.1039/C3CP52459K (2013).
49. Chen, J. & Xiang, L. Controllable synthesis of calcium carbonate polymorphs at different temperatures. *Powder Technol.* **189**, 64–69. https://doi.org/10.1016/j.powtec.2008.06.004 (2009).

Acknowledgements
The authors gratefully acknowledge financial support from the Sumitomo Foundation (No. 203137) and the Japan Society for the Promotion of Science (JSPS, 21K14571). The authors thank Dr. Shinichi Yamasaki for assistance with ICP-OES analysis of the fluids. We would like to thank Editage (www.editage.com) for English language editing.

Author contributions
Conceptualization, N.W. and J.W.; Data curation, J.W.; Formal analysis, J.W. and N.W.; Funding acquisition, J.W., N.W. and N.T.; Investigation, J.W., N.W. and K.I.; Methodology, J.W. and, N.W.; Project administration, J.W.; Resources, N.W. and K.N.; Supervision, N.T. and T.K.; Validation, J.W.; Visualization, J.W. and N.W.; Writing—original draft, J.W.; Writing—review & editing, N.W., M.K. and N.T. All authors have read and agreed to the published version of the manuscript.

Competing interests
The authors declare no competing interests.

Additional information
Correspondence and requests for materials should be addressed to J.W. or N.W.

Reprints and permissions information is available at www.nature.com/reprints.

Publisher's note Springer Nature remains neutral with regard to jurisdictional claims in published maps and institutional affiliations.